JOURNAL OF CATALYSIS **172,** 414–426 (1997)
ARTICLE NO. CA971847

Amorphous Sn/Si Mixed Oxides, Mild Solid Lewis Acid Catalysts for Esterification and Etherification Reactions

S. Storck,* W. F. Maier,*,[1] I. M. Miranda Salvado,† J. M. F. Ferreira,† D. Guhl,‡ W. Souverijns,§ and J. A. Martens§

*Max-Planck-Institut für Kohlenforschung, Mülheim an der Ruhr, Germany; †DECV, Universidade de Aveiro, Aveiro, Portugal; ‡Th. Goldschmidt AG, Mannheim, Germany; and §Centrum voor Oppervlaktechemie en Katalyse, KU Leuven, Leuven, Belgium

Received March 17, 1997; revised July 4, 1997; accepted July 22, 1997

Novel amorphous porous mixed oxides of Sn, Si, and Al were prepared by the sol–gel process for use as solid acid catalysts. The materials were characterized by XRD, HRTEM, SEM, EDX, argon-physisorption, DRIFTS, and pyridine adsorption followed by FTIR. The catalysts show very few Brønsted sites and some Lewis acid sites. The pore architecture of the materials was studied by the hydrocracking test of decane which indicated weak activity but clear shape selectivity for most of the mixed oxides. Further catalytic testing included the direct esterification reaction of pentaerythritol with stearic acid to pentaerythritoltetrastearate and the etherification of 1-hexanol and 1-naphthol with isobutene. The esterification reaction was studied under reaction conditions close to industrial ones. The catalysts were found to be as active as commercial homogeneous and heterogeneous catalysts. While the activity found in the esterification reaction can be correlated with the increase in surface area and the decrease in Sn content, no correlation with microstructural parameters was found in the etherification reactions.

INTRODUCTION

Solid acid catalysts are of increasing importance for esterification and etherification reactions in the production of bulk and fine chemicals (1, 2). Such heterogeneous catalysts offer several advantages over traditional homogeneous catalysts in chemical production: insolubility in the product, reusability, increased product purity, and reduction of the cost of purification. To be of economical interest, the heterogeneous catalysts should be of comparable activity and selectivity. Most solid acid literature is concerned with strongly acidic materials suitable for hydrocarbon isomerization and cracking in the petrochemical industry (3). Although heterogeneous catalysts have become increasingly interesting for esterification and transesterification reactions (4, 5), little is known about the properties of Sn-containing amorphous mixed oxides as solid acid catalysts. In the past, sulfated zirconia as well as heteropolyacids were mainly used as superacid catalysts in esterification reactions (6).

Pure SnO_2 is an amphoteric material. In the conversion of propane-2-ol to acetone its basic properties are utilized (7). Its solid acid properties are shown in the isomerization of cyclopropane (8) and 1-butene (9) as well as in the dehydrogenation of cyclohexanol to cyclohexanone (10). The acid strength of SnO_2 can be so strongly enhanced by the addition of sulfate ions (8, 10) that it catalyzes the skeletal isomerization of butane at room temperature (11). The acid strength of the Zr/Sn mixed oxide system can be increased by adding sulfate ions, as shown in the isomerization reaction of *n*-butane to isobutane (7). Several Sn-containing catalyst systems, including TiO_2–SnO_2 (9, 12), ZrO_2–SnO_2 (7, 13), CeO_2–SnO_2, and Ln_2O_3–SnO_2 (13) were recently studied.

Little is known about the catalytic properties of Sn-containing mixed oxides based on silica or alumina. Mixing oxides often generates new acid sites or modulates the acid properties of the bulk oxides. Several theories (14) have been introduced to predict the enhanced acidity of mixed oxides and to explain their high activity in acid catalyzed reactions. Surface acidity has been predicted for the Si/Sn system (15).

This work explores the catalytic properties of Sn/Si, Sn/Al, Sn/Si/Al, and Al/Si mixed oxides in esterification and etherification reactions with emphasis on the Sn/Si-mixed oxides. Al was added in selected samples as a "reference" component, since the Brønsted-acidic aluminum silicates belong to the best studied solid acids (16). Since little is known about the Sn/Al and Si/Sn/Al systems, the effect of Al in these mixed oxides on textural, structural, and catalytic properties was also investigated.

The sol–gel process is an attractive, mild procedure for the controlled preparation of porous mixed oxides (17, 18). An inorganic polymer network is formed via hydrolysis and condensation of metal salts and alkoxides. The chemical composition of mixed oxides prepared by the

[1] Corresponding author. E-mail: maier@mpi-muelheim.mpg.de.

0021-9517/97 $25.00

sol–gel process can be controlled by the stoichiometry of the sol-composition. The first silicon–tin mixed oxide materials have already been prepared by sol–gel procedures (19–22). It has recently been shown that domain-free Ti- and V-containing amorphous microporous silicon oxides, prepared by a modified sol–gel method, have a very narrow micropore distribution. These materials are not only catalytically active solid acids (23), but also shape selective catalysts in hydrocracking reactions (24). The micropore system of these materials is formed during the drying and calcination procedure (25). The method allows the formation of domain-free mixed oxides, as shown with Ti–Si-containing catalysts (23). Sol–gel processes were, therefore, selected for the preparation of the Sn-containing porous mixed oxides of various compositions. So far only a few examples of shape selective tin-containing materials have been reported. Crystalline Sn-silicalites with an MFI-structure have been found to be catalytically active in partial oxidation reactions of organic substrates (26–28).

Here we report the preparation and application of new mild solid acids based on Sn–Si mixed oxides as suitable catalysts for esterification and etherification reactions. The catalysts were tested in the synthesis of a technically relevant ester, and their activity was compared with traditional homogeneous catalysts. We will describe the preparation and characterization of mixed metal oxides with different amounts of Sn, Al, and Si. Due to the different laboratories involved, two preparation procedures were applied. The characterization focuses on the surface area, the pore architecture, the acidity, and the microstructure of the different materials on a molecular scale. The potential of the materials to act as acidic and molecular shape-selective catalysts was examined by the hydrocracking reaction of decane (29). The esterification reaction of pentaerythritol with stearic acid was selected as a test reaction in view of its industrial importance. Further catalytic tests included the etherification of 1-hexanol and 1-naphthol with isobutene to the corresponding *t*-butylethers.

EXPERIMENTAL

Catalyst Preparation

The mixed oxides were prepared by acid catalyzed sol–gel methods. Silicon alkoxides and aluminum salts were mixed with tin precursors and alcohols. Drying and calcination of the gel under controlled conditions led to amorphous, highly porous materials. For simplification, the materials will be referred to as AO–$Sn_xAl_ySi_z$, where AO stands for amorphous oxides with the subscript numbers indicating the atomic percentage of the respective elements.

Since two research groups with different experience and background in sol–gel chemistry were involved in the synthesis of the AO-materials, two strategies were applied to obtain the gels. The synthesis of the amorphous oxides AO–$Sn_{25}Al_{36}Si_{39}$, AO–$Al_{48}Si_{52}$, AO–$Sn_{25}Al_{75}$, and AO–$Sn_{13}Si_{87}$ was carried out according to method I. Si and Al precursors were mixed with the alcohol component prior to the addition of the tin component. The gels were then dried at 60°C followed by calcination at 550°C.

In contrast, the materials AO–Sn_4Si_{96}, AO–$Sn_{12}Si_{88}$, AO–$Sn_{20}Si_{80}$, and AO–Si_{100} were prepared according to method II. All alkoxide components were mixed prior to adding the alcohol. For hydrolysis and condensation the Sn containing gels were kept at 40°C. Aging at 20°C was followed by calcination at 250°C.

All sols were prepared by means of magnetic stirring, which stops as the gel point is approached. Although some of the gels have similar chemical compositions, differences in textural and structural properties are attributed to the different preparation and drying methods.

Preparation of the Catalysts AO–$Sn_{25}Al_{36}Si_{39}$, AO–$Al_{48}Si_{52}$, AO–$Sn_{25}Al_{75}$, and AO–$Sn_{13}Si_{87}$ (Method I)

AO–$Al_{48}Si_{52}$ was prepared by mixing 55.63 g (0.148 mol) aluminum nitrate nonahydrate dissolved in 111.3 ml (1.906 mol) absolute ethanol (minimum amount necessary to dissolve the nitrate) with 9.1 ml (40.7 mmol) tetraethoxysilane, 2.5 ml (0.138 mol) distilled water, and 0.68 ml (8.185 mmol) aqueous HCl (12.5 M).

AO–$Sn_{25}Al_{36}Si_{39}$ was prepared by adding 10.09 g (24.91 mmol) tin (II)-2-ethylhexanoate to an alumina–silica sol prepared as described above.

AO–$Sn_{25}Al_{75}$ was prepared by adding 9.00 g (22.21 mmol) tin (II)-2-ethylhexanoate to an alumina sol prepared by mixing 66.20 g (0.176 mol) aluminum nitrate nonahydrate with 132.0 ml (2.260 mol) absolute ethanol, 2.5 ml (0.183 mol) distilled water, and 0.68 ml (8.185 mmol) aqueous HCl (12.5 M).

AO–$Sn_{13}Si_{87}$ was prepared by adding 9.00 g (22.21 mmol) tin (II)-2-ethylhexanoate to a silica sol prepared by mixing 33.6 ml (0.150 mol) tetraethoxysilane with 111.3 ml (1.906 mol) absolute ethanol, 2.5 ml (0.138 mol) distilled water, and 0.68 ml (8.185 mmol) aqueous HCl (12.5 M). The final sols were kept in glass containers covered with polyethylene foil at 60°C until gelation. After aging for one week at 60°C the obtained gels were dried for 24 h at 120°C and heat treated at 550°C for 5.5 h in air.

Preparation of the Catalysts AO–Sn_4Si_{96}, AO–$Sn_{12}Si_{88}$, AO–$Sn_{20}Si_{80}$, and AO–Si_{100} (Method II)

AO–Sn_4Si_{96} was prepared by mixing 5.55 g (13.7 mmol) tin (II)-2-ethylhexanoate with 70.00 ml (313 mmol) tetraethoxysilane in a 250 ml polypropylene Erlenmeyer flask under argon. After 15 min 50.6 ml (862 mmol) ethanol were added to the solution. The sol was hydrolyzed with 8.4 ml (101 mmol) aqueous HCl (12.5 M) and 4.1 ml (229 mmol)

H_2O. The solution was stirred for 24 h under argon at 40°C. The gel was left in the open flask for 22 days until a clear monolith formed. The monolith was placed in an open ceramic dish and dried at 20°C for 7 days, followed by calcination at 250°C in air.

AO–$Sn_{20}Si_{80}$ was prepared by mixing 113.3 ml (507 mmol) tetraethoxysilane with 103.0 ml (1.75 mol) ethanol for 20 min in a large beaker. 33.8 ml (126 mmol) di-*n*-butyldiacetoxytin were added dropwise to the solution. The resulting sol was kept at 40°C for 7 days. After one more day at 20°C the gelation process was completed. The gel was dried at 20°C for 7 days and calcined at 250°C in air.

AO–$Sn_{12}Si_{88}$ was prepared by adding 19.5 ml (185 mmol) 1,1,1,3,3,3-hexafluoro-2-propanol and 47.8 ml (815 mmol) ethanol to 75.0 ml (336 mmol) tetraethoxysilane. 11.2 ml (41.9 mmol) di-*n*-butyldiacetoxytin was added dropwise to the solution. The workup was identical to AO–$Sn_{20}Si_{80}$.

AO–Si_{100} was prepared by mixing 15.0 ml (67.2 mmol) tetraethoxysilane with 11.8 ml (202 mmol) ethanol in a 100 ml polypropylene beaker. The sol was hydrolyzed with 2.0 ml (24 mmol) aqueous HCl (12.5 M) and 1.0 ml (53 mmol) H_2O. The solution was strirred for 24 h at 25°C. The gel was left in the open beaker for 5 days until a clear monolith formed. The monolith was placed in an open ceramic dish and dried at 20°C for 3 days, followed by calcination at 250°C in air.

CATALYST CHARACTERIZATION

X-Ray Diffraction

X-ray powder diffraction (XRD) patterns were measured using the Debye–Scherrer technique on a Stoe Stadi 2/PL diffractometer with Cu Kα radiation in the range of $2\theta = 10$–80° and the area detector PSD 1. All powdered gels were studied at room temperature after calcination.

Electron Microscopy

The bulk appearance of the materials was studied by scanning electron microscopy (SEM) using a Hitachi S 4100 microscope equipped with a Quantum Kevex Model No. 3600-0615 EDX facility. For sample preparation the powders were suspended in ethanol, treated by ultrasound, deposited on a microscope sample holder, and coated with a thin carbon film.

A Hitachi HF-2000 (acceleration voltage 200 keV) was used for high resolution transmission electron microscopy (HRTEM). Energy dispersive X-ray analysis (EDX) was performed using a Noran EDX-system with a liquid nitrogen cooled Si (Li)-detector. For sample preparation the catalyst powders were ground, suspended in methanol, and deposited on Holey-carbon-grids (Cu, 400 mesh, 3 mm diameter).

Physisorption

Adsorption isotherms of the catalysts were collected with argon physisorption in liquid argon (30) with an Omnisorp 360 instrument from Coulter. Samples were outgassed for 12 h at 250°C prior to adsorption. B.E.T. specific surface areas and micropore size distributions, according to the Horvath Kawazoe (31) method using the nitrogen on carbon potential and mesopore distributions based on the Kelvin equation, were obtained from the isotherms using the ADP software version 3.0.2 from Porotec.

Infrared Spectroscopy

Fourier transform infrared transmission spectra (FTIR) of the different AO-materials were collected with a Bruker IFS 48 Fourier transform spectrometer with a spectral resolution of 2 cm^{-1} at 200 scans. For DRIFTS measurements the AO-materials were dried *in situ* at 400°C for 12 h in a flow of dry argon using a reaction chamber (Harrick HVC) in combination with a diffuse reflectance unit (Harrick DRA-XX). Spectra were collected at 30°C, and the experimental data were displayed using the Kubelka Munk function (dry KBr as background). For surface acidity DRIFTS measurements the samples were dried according to the method explained above. Subsequently a stream of argon saturated with dry pyridine (distilled and stored over KOH) was purged through the cell over the sample for 30 min at 80°C. The excess of physisorbed pyridine was removed in a flow of dry argon at 120°C for 30 min. The spectra were taken at 120°C and displayed using the Kubelka Munk function (pure AO material spectrum as background).

The surface acidity was measured in transmission mode by means of FTIR spectroscopy after adsorption of pyridine as a probe molecule. Five milligrams of the sample were exposed to pyridine vapor in a flow of argon at 80°C for 1 h. To remove surface bound pyridine species, the sample was finally kept under a flow of argon at 120°C for 1 h. To record the spectra, the sample was placed between KBr discs in poly-(chloro-trifluorethylene)-oil. The resulting spectrum was baseline corrected.

CATALYTIC TESTING

Synthesis of Pentaerythritoltetrastearate

In a 1 1 4-necked round-bottom flask, equipped with a distillation bridge, thermometer, mechanical stirrer, gas inlet, and heating device, 284.5 g (1.0 mol) stearic acid was molten at 55°C under a steady flow of nitrogen; then 40.9 g (0.3 mol) pentaerythritol and the catalyst (0.1, or 0.4 wt% relative to formulation) were added. The temperature was slowly increased to 170–200°C in order to minimize losses of pentaerythritol due to sublimation. Distillation of the reaction water started at 150–170°C. Beginning with the first drop of water in the distillation flask, a sample was taken

from the reaction mixture every hour, and its acid value was determined by titration with potassiumhydroxide solution according to DIN 53402. The reaction was stopped when no significant change in the acid value occurred after 2 h. The particle size of the AO-materials used was smaller than 50 μm. In a control experiment no water could be condensed in the absence of the catalyst for 5 h, indicating no or a weak reaction.

Etherification

The competitive etherification of 1-hexanol and 1-naphthol was performed in a 200-ml stainless steel high pressure reaction vessel. Twenty-seven milliliters (300 mmol) isobutene, 7.21 g (50 mmol) 1-naphthol, and 5.11 g (50 mmol) 1-hexanol were mixed with the catalyst (300 mg) under argon. The vessel was closed and pressurized to 3.0×10^6 Nm^{-2} with nitrogen. The solution was stirred with a magnetic stirrer and heated to 140°C for 17 h. At the end of the reaction the vessel was depressurized and the catalyst was removed from the solution. Samples of the solution were taken and analyzed by gas chromatography.

Decane Test

Decane isomerization and hydrocracking were performed in a continuous-flow, fixed-bed vapor phase reactor as described previously (24). The amorphous oxide samples were converted into bifunctional catalysts by loading them with a trace of platinum metal (0.1 or 0.5 wt%). The gel samples were impregnated with an aqueous solution of $Pt(NH_3)_4Cl_2$, according to the incipient wetness technique. The gel powders were shaped into pellets with diameters from 0.25 to 0.50 mm by compression, crushing, and sieving. The catalyst bed was activated by oxidation at 400°C in a stream of oxygen followed by reduction in flowing hydrogen at the same temperature. Decane vapor (partial pressure 1 kPa) in hydrogen (partial pressure 450 kPa) was converted at a space time of 0.5 kg h mol^{-1}. The conversion of decane was changed stepwise by the reaction temperature.

RESULTS AND DISCUSSION

Catalyst Characterization

X-Ray Diffraction

To prove the amorphous character of the calcined gels, XRD analysis was carried out on all calcined samples. For AO–$Sn_{13}Si_{87}$ cassiterite patterns appear, indicating the presence of a tetragonal SnO_2 phase in this mixed oxide prepared according to method I (Fig. 1). The binary Sn/Al and Al/Si mixed oxides and the ternary Sn/Al/Si system appear to be X-ray amorphous. The X-ray amorphous character of the Al-containing gels, prepared according to method I, leads to the conclusion that the crystallization process of Sn in the Sn/Si mixed oxide system is suppressed by the

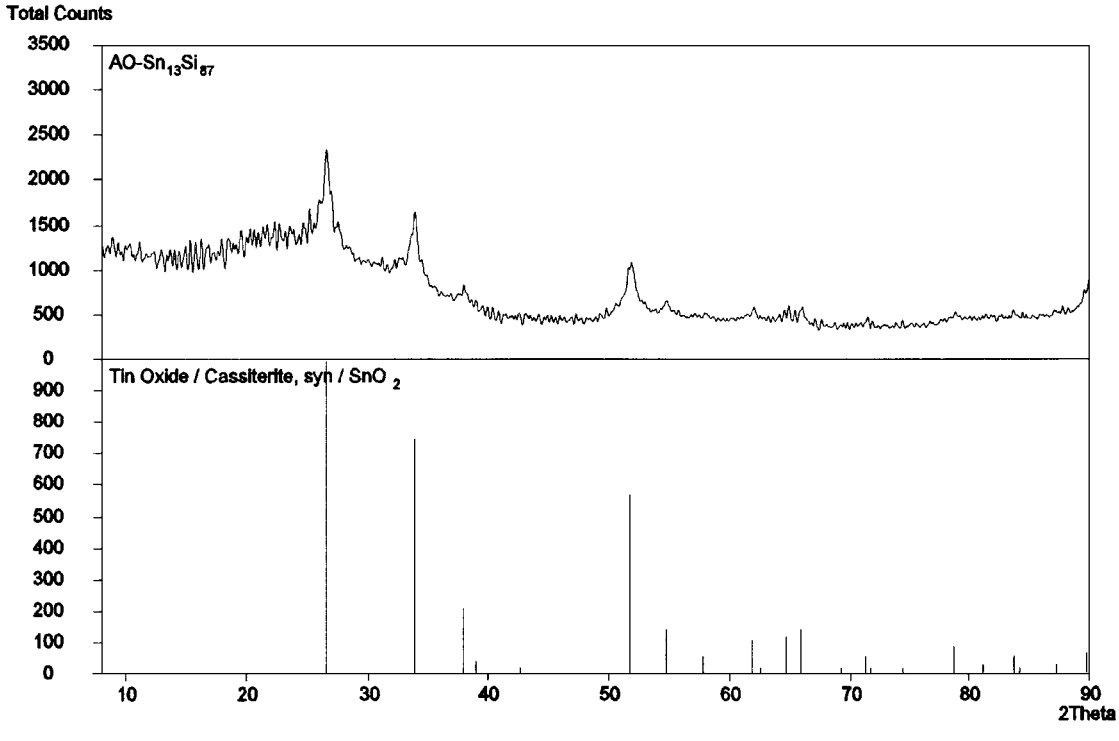

FIG. 1. XRD patterns of AO–$Sn_{13}Si_{87}$, together with a cassiterite reference spectrum.

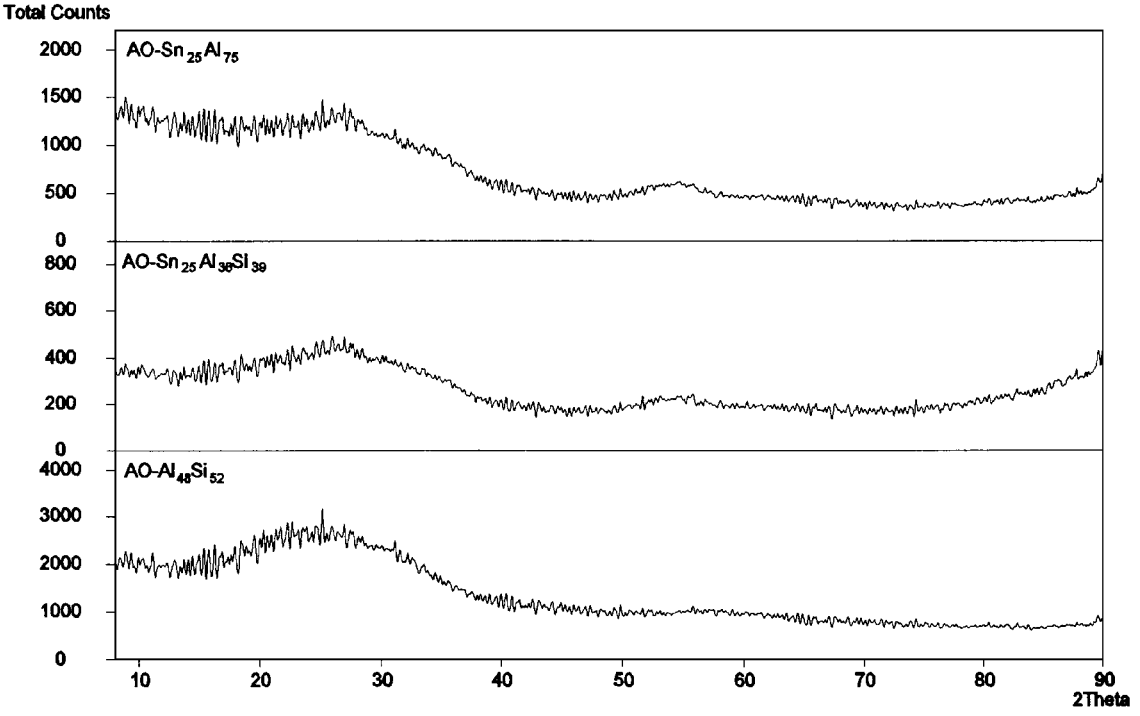

FIG. 2. XRD patterns of the binary and ternary Al-containing AO materials prepared according to method I.

addition of Al (Fig. 2). The use of preparation method II leads to X-ray amorphous Sn/Si systems (AO–Sn_4Si_{96}, AO–$Sn_{12}Si_{88}$, and AO–$Sn_{20}Si_{80}$) with a high tin content, without the addition of Al (Fig. 3).

Electron Microscopy (SEM/EDX)

Scanning electron microscopy (SEM) and energy dispersive X-ray analysis (EDX) were carried out with all

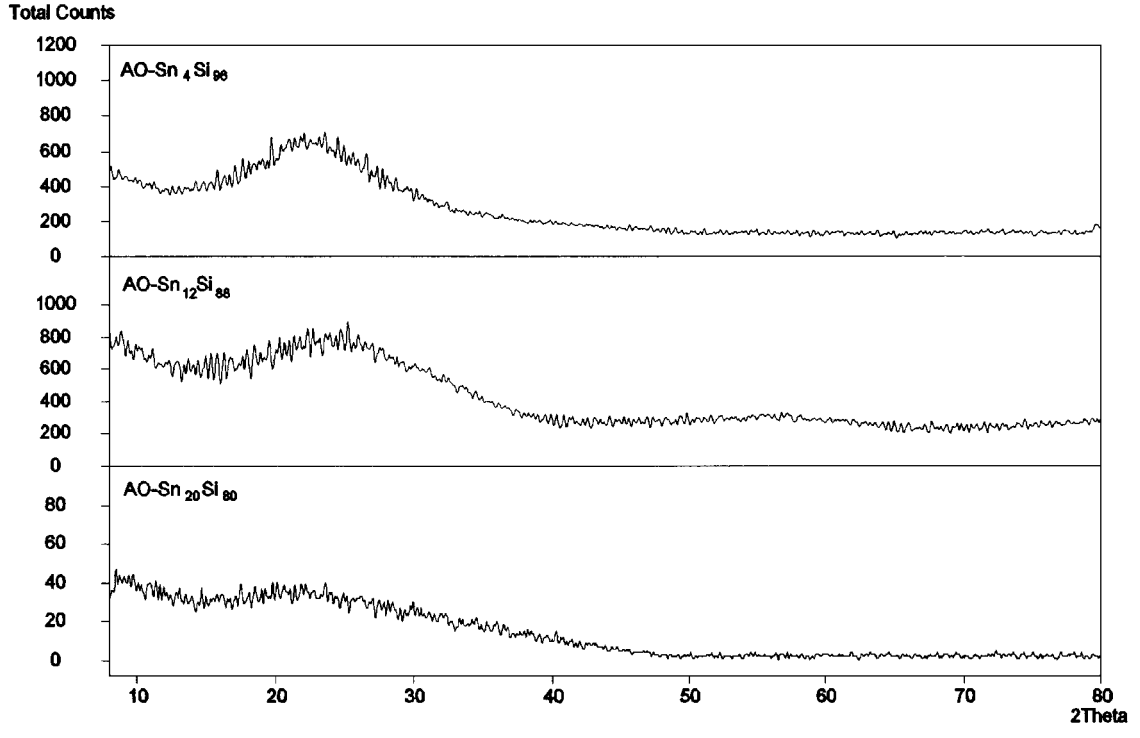

FIG. 3. XRD patterns of the binary Sn/Si mixed oxide systems prepared according to method II.

powdered samples. EDX analysis was made on all samples at 10 k magnification. The accuracy of the analysis is lower for a powdered material than for polished surfaces. Nevertheless, the EDX results provide valuable evidence for the chemical homogeneity of the materials.

Powdered samples of AO–Sn_4Si_{96}, AO–$Sn_{20}Si_{80}$, and AO–$Sn_{12}Si_{88}$ have very similar morphologies. They appear as a glass-like material with particles of different sizes. According to the elemental mapping for Si and Sn they can be considered to have homogeneous elemental distribution without domain formation, in confirmation of the XRD results.

AO–$Sn_{13}Si_{87}$ shows separated zones of SnO_2 and SiO_2. The sample appears to be a porous block with fracture areas typical of glass-like materials. AO–$Sn_{25}Al_{75}$ consists of a continuous phase with fractures due to the heat treatment. No domain formation of Al or Sn was detected (Fig. 4). In sample AO–$Sn_{25}Al_{36}Si_{39}$ and AO–$Al_{48}Si_{52}$ no phase separation of the oxides was detected. They appear as homogeneous mixed oxides.

The SEM results confirm the XRD experiments. The studies indicate that only AO–$Sn_{13}Si_{87}$ contains domains of tetragonal SnO_2. All other samples are homogeneous mixed oxides at this magnification. Preparation method II, used for the Sn/Si mixed oxides AO–Sn_4Si_{96}, AO–$Sn_{20}Si_{80}$, and AO–$Sn_{12}Si_{88}$, seems to lead to domain-free gels. For materials containing Al, the premixing of Si and Al precursors, as indicated in method I, seems to be the appropriate method for obtaining homogeneous mixed Al oxides.

Electron Microscopy (HRTEM/EDX)

Investigations of the textural properties of the materials at atomic resolution, carried out with high-resolution transmission electron microscopy (HRTEM) and EDX, give a more detailed picture of the Sn/Si system prepared according to method II. AO–$Sn_{20}Si_{80}$ appeared to be nonhomogeneous and partially microcrystalline. Tin-enriched spherical crystallites embedded in an amorphous silica matrix were detected (Fig. 5). AO–Sn_4Si_{96} was completely homogeneous and amorphous (Fig. 6). It seems that there is a clear limit to the amout of tin that can be incorporated homogeneously into the silica network using the sol–gel route II. The described investigations indicate that a highly dispersed Sn/Si mixed oxide can be obtained using up to 4% tin with preparation method II.

The ternary system $Sn_{25}Al_{36}Si_{39}$, prepared according to method I, appeared to be nonhomogeneous and partially microcrystalline at atomic resolution. Alumina-enriched domains, embedded in an amorphous matrix, were found. The atomic percentages found by the EDX analyses correlate with the amount used in the preparation of the samples.

Physisorption

The argon adsorption isotherms are shown in Fig. 7. AO–Sn_4Si_{96}, AO–Si_{100}, AO–$Sn_{13}Si_{87}$, $Sn_{12}Si_{88}$, and AO–$Sn_{20}Si_{80}$

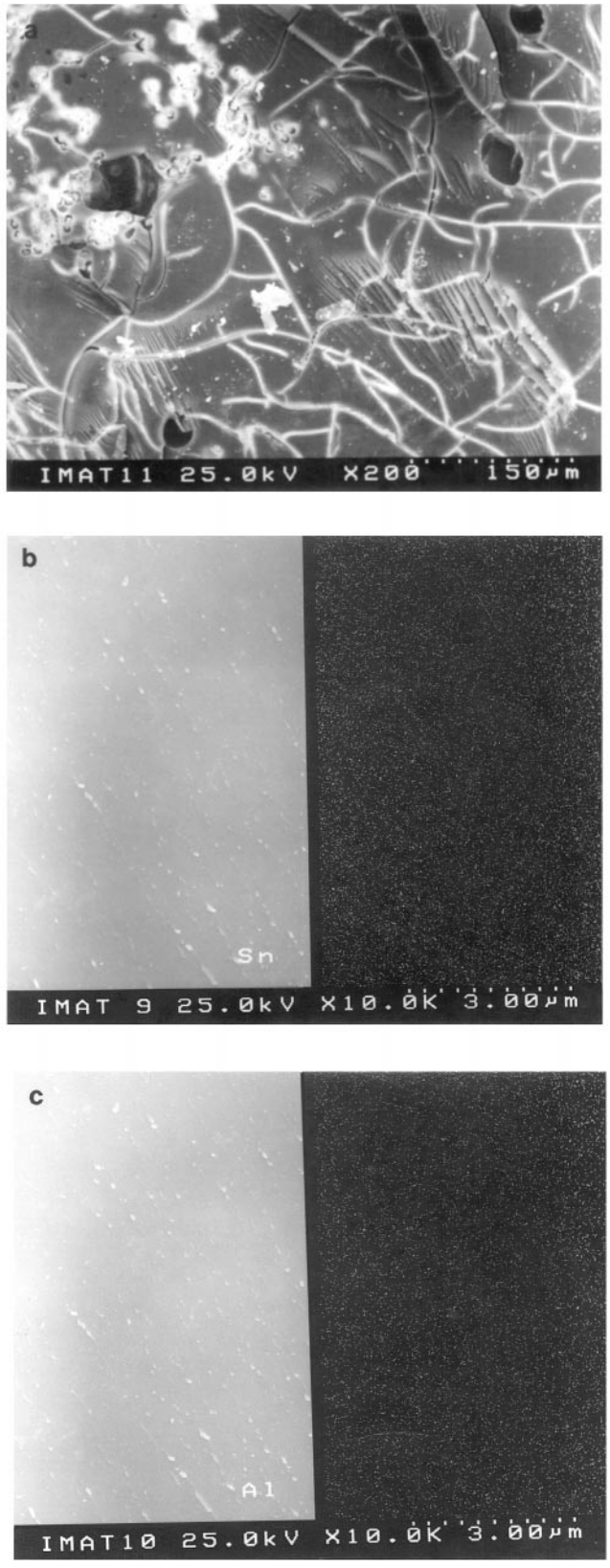

FIG. 4. SEM micrographs of sample AO–$Sn_{25}Al_{75}$. (a) Structure of the material. (b) Selected area of the sample with the corresponding Sn elemental distribution. (c) Selected area of the sample with the corresponding Al elemental distribution.

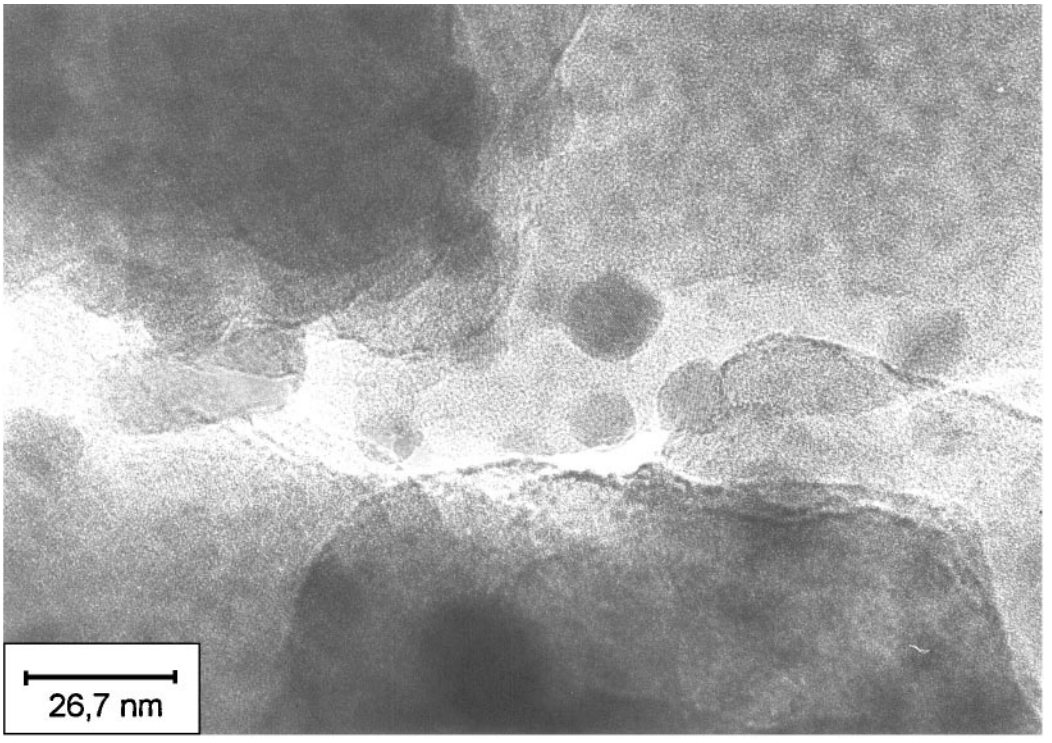

FIG. 5. HRTEM micrograph of sample AO–$Sn_{20}Si_{80}$ with spherical crystallites embedded in an amorphous silica matrix.

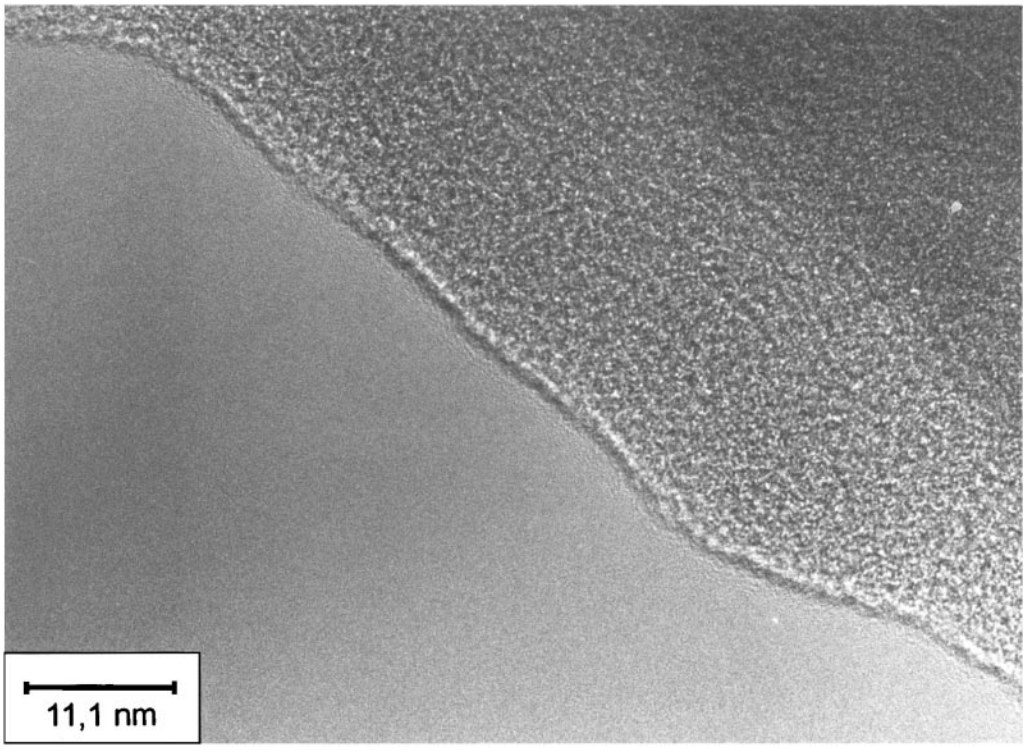

FIG. 6. HRTEM micrograph of sample AO–Sn_4Si_{96} shows a completely amorphous material.

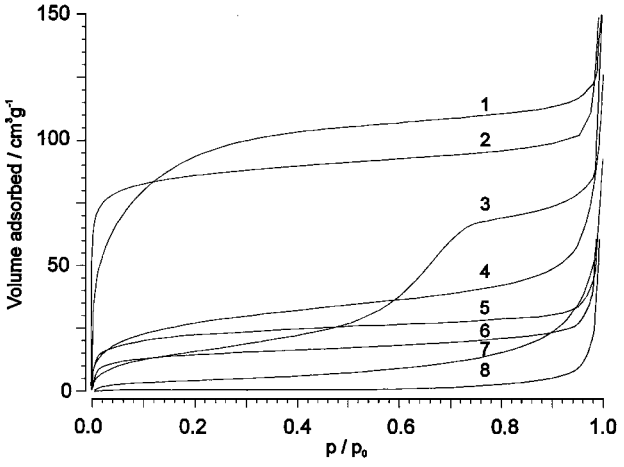

FIG. 7. Argon physisorption isotherms: 1, AO–Sn_4Si_{96}; 2, AO–Si_{100}; 3, AO–$Sn_{25}Al_{75}$; 4, AO–$Sn_{13}Si_{87}$; 5, AO–$Sn_{12}Si_{88}$; 6, AO–$Sn_{20}Si_{80}$; 7, AO–$Sn_{25}Al_{36}Si_{39}$; 8, AO–$Al_{48}Si_{52}$.

have isotherms of type I, indicative of microporosity. AO–$Sn_{25}Al_{36}Si_{39}$ and AO–$Al_{48}Si_{52}$ have adsorption isotherms of type III, corresponding to external adsorption outside micro- and mesopores. For AO–$Sn_{25}Al_{75}$, the isotherm type IV indicates the presence of mesopores.

Specific surface areas were determined from these isotherms, adopting the B.E.T. formalism. Strictly speaking, the B.E.T. model is applicable to types II and IV isotherms only. The values derived for the other isotherm shapes (Table 1) should be interpreted with caution. Clear correlations between the surface area, metal content, and preparation method can be seen. For AO materials prepared according to method II, the addition of 4% tin precursor in the sol–gel process does not lead to significant changes in the surface area of the SiO_2 system. AO–Si_{100} and AO–Sn_4Si_{96} show almost identical surface areas. Larger amounts of the metal used in AO–$Sn_{12}Si_{88}$, AO–$Sn_{20}Si_{80}$, and AO–$Sn_{13}Si_{87}$ lead to lower surface areas, independently of the preparation method used. In the course of AO material preparation according to method I, the role of Al in the Si/Sn mixed oxides was investigated. The binary and the ternary systems, AO–$Al_{48}Si_{52}$ and AO–$Sn_{25}Al_{36}Si_{39}$, exhibit low surface areas consisting of micropores, while the Sn/Al mixed oxide shows mainly mesopores. In order to draw detailed conclusions about the role of Al in the mixed oxides, additional studies of the influence of the Al content in these mixed metal oxides are necessary.

TABLE 1

Physisorption Results of AO-Catalysts

Sample	Mean pore diameter [nm]	B.E.T. surface area [m^2/g]	Cumulative micropore volume [ml/g]
AO–Sn_4Si_{96}	0.64	308	0.144
AO–$Sn_{13}Si_{87}$	0.57	88	0.069
AO–$Sn_{12}Si_{88}$	0.74	73	0.039
AO–$Sn_{25}Al_{75}$	5.34	53	0.098
AO–$Sn_{20}Si_{80}$	0.70	48	0.032
AO–Sn_{25} $Al_{36}Si_{39}$	0.87	15	0.035
AO–$Al_{48}Si_{52}$	—	4	—
AO–Si_{100}	0.72	300	0.127

For the microporous materials, modeling the energies of the adsorption process, using Lennard–Jones potential energy functions, can be used to determine pore size distributions and to distinguish small differences in pore diameters (32, 33). The main micropore diameters obtained by the Horvath–Kavazoe (31) approach, assuming all-silica surfaces, are listed in Table 1. The micropore distributions of the amorphous AO-materials are generally broader than in crystalline zeolite material, and the cumulative micropore volumes are smaller. The main pore diameters are in the range of 0.57 to 0.87 nm, which is the range of the micropore diameters encountered in silica-based zeolites. The main pore diameter in the AO–$Sn_{25}Al_{75}$ sample, derived from the type IV isotherm using the Kelvin equation, is 5.3 nm. Since the micropore volumes are rather low, a detailed discussion of the pore size distribution in relation to the preparation method and metal content is not justified.

Infrared Spectroscopy

Pyridine was used as the probe molecule for analysis of the surface acidity of the amorphous oxides by FTIR spectroscopy in the transmission mode (34). This technique allows a clear distinction between Brønsted and Lewis acid sites. The absorption band at 1540 cm^{-1} is attributed to the pyridinium ion formed by adsorption on Brønsted sites, while pyridine coordinated to Lewis sites shows absorptions at 1605, 1580, and 1450 cm^{-1} (7, 35). The latter is not considered, due to possible interference with signals attributed to pyridine coordinated to nonacidic OH functions. AO–Si_{100}, AO–$Sn_{25}Al_{75}$, AO–$Sn_{25}Al_{75}Si_{39}$, AO–Sn_4Si_{96}, and AO–$Sn_{13}Si_{87}$ exhibit intense nonacidic silanol bands (1450 and 1595 cm^{-1}). They indicate a high density of polar silanol groups present in the materials. Weak absorption bands, indicative of Lewis sites, are present only in the materials AO–$Sn_{25}Al_{75}$, AO–$Sn_{25}Al_{36}Si_{39}$, and AO–Sn_4Si_{96} (Fig. 8). Indications of weak Brønsted sites were found in the materials AO–$Sn_{25}Al_{75}$ and AO–$Sn_{25}Al_{36}Si_{39}$. All other samples show virtually no acidity.

To complement the transmission spectra, the analyses were repeated with all samples using an *in situ* preparation technique for the pyridine adsorption, followed by DRIFTS measurements. DRIFTS was not suitable for these materials due to very low reflectance of the samples, leading to a loss of information in the spectra. No signals due to acidic sites could be identified in the samples.

Sn-containing silicalite and Sn/Si mixed oxides with a high Sn content exhibit an IR absorption at 950–980 cm^{-1}. This band has been attributed to the presence of Si–O–Sn

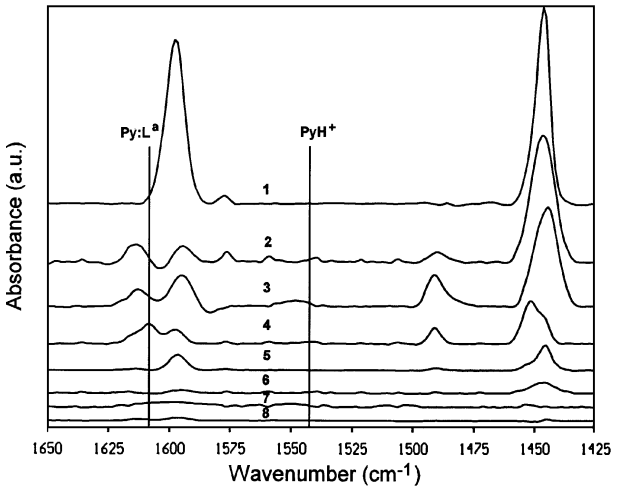

FIG. 8. FTIR absorbance spectra of AO materials after pyridine adsorption. 1, AO–Si_{100}; 2, AO–$Sn_{25}Al_{75}$; 3, AO–$Sn_{25}Al_{36}Si_{39}$; 4, AO–Sn_4Si_{96}; 5, AO–$Sn_{13}Si_{87}$; 6, AO–$Sn_{12}Si_{88}$; 7, AO–$Sn_{20}Si_{80}$, 8, AO–$Al_{48}Si_{52}$.

linkages (26, 27, 19). The 950–980 cm^{-1} band, however, is absent in the IR-spectra of other dehydrated Sn–Si oxides (21, 36). The authors do not give information about the pretreatment of the catalysts prior to measurement, so that it is not possible to distinguish between bands of possible Si–O–Sn linkages or bands of surface Si–OH groups. The spectral features of the AO-materials were investigated with FTIR-spectroscopy in the diffuse reflectance mode (DRIFT). To avoid confusion with the dominating surface Si–OH groups (920–960 cm^{-1}), the AO-samples had to be heat treated at 400°C in a dry atmosphere prior to the measurement. The DRIFT spectra of the heat-treated Si/Sn/Al mixed oxides are shown in Fig. 9, clearly demonstrating the absence of a band at 950–980 cm^{-1}. We assume that the absence of this band is caused by Sn coordination higher than tetrahedral due to the coordination of water and/or alcohol. Similar effects have been reported for the Si–Ti system with a band at 950 cm^{-1} attribute to Si–O–Ti vibrations of tetrahedral Ti (23).

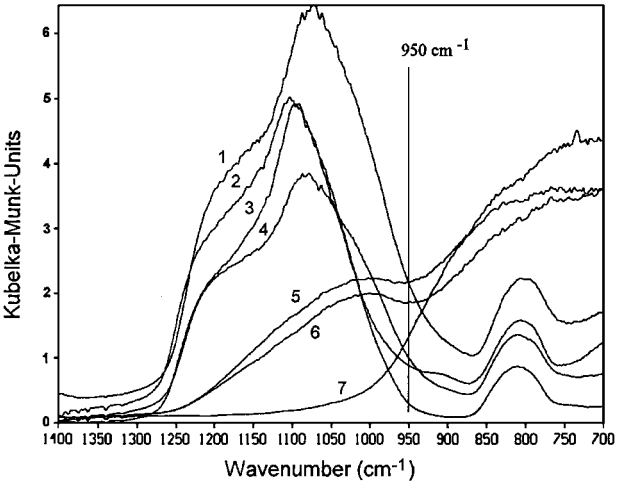

FIG. 9. DRIFT spectra of heat treated AO-materials. 1, AO–$Sn_{20}Si_{80}$; 2, AO–$Sn_{13}Si_{87}$; 3, AO–Sn_4Si_{96}; 4, AO–$Sn_{12}Si_{88}$; 5, AO–$Al_{48}Si_{52}$; 6, AO–$Sn_{25}Al_{36}Si_{39}$; 7, AO–$Sn_{25}Al_{75}$.

TABLE 2

Comparison of Catalytic Esterification with Homogeneous Catalysts

Catalyst	Amount [%]	Acid value [mg KOH/g] after reaction time 3 h	4 h	5 h
$(C_4H_9)_2SnO$	1	12.8	7.3	2.9
SnO	0.1	4.7	4.6	4.2
SnC_2O_4	0.1	7.6	7.3	—
ZnO	0.1	8.5	6.9	—
$Ti(OC_4H_9)_4$	0.1	22.6	17.5	13.2

Catalytic Testing

Esterification

The amorphous AO catalysts were tested under reaction conditions close to technical procedures in the direct esterification reaction of pentaerythritol and stearic acid to pentaerythritoltetrastearate. In order to obtain data on the efficiency of the state of the art of homogeneous catalysts, several experiments were run with commercial homogeneous catalysts. In addition, commercial heterogeneous catalysts were evaluated together with the new Sn/Al/Si mixed oxides. The results of the homogeneous catalysts are shown in Table 2. The commercial catalysts were used without pretreatment. The use of di-*n*-butyltin oxide led to the product with the lowest content of free fatty acids and an ester yield of 98.5%.

Tin (II) oxide showed the highest catalytic activity among the samples tested. Low acid values are achieved during 3 h reaction time, without further significant decreases during the next 2 h. The performance of two tin-free products is shown in Table 3. The results indicate that these materials did not reach the catalytic activity of the best homogeneous

TABLE 3

Comparison of Catalytic Esterification on Tin-Free Commercial Heterogeneous Catalysts

Catalyst	Amount [%]	Acid value [mg KOH/g] after reaction time 3 h	4 h	5 h
SO_4/ZrO_2	0.4	18.1	14.2	11.5
Filtrol 24	0.4	19.8	15.4	12.7

TABLE 4

Comparison of Catalytic Esterification with AO-Materials

Catalyst	Amount [%]	Acid value [mg KOH/g] after reaction time 3 h	4 h	5 h
AO–$Sn_{13}Si_{87}$	0.4	12.6	9.8	5.6
AO–Sn_4Si_{96}	0.4	8.7	7.3	—
AO–$Sn_{12}Si_{88}$	0.4	16.9	12.5	8.1
AO–$Sn_{20}Si_{80}$	0.4	17.5	12.8	9.1
AO–$Sn_{25}Al_{36}Si_{39}$	0.4	18.4	12.2	10.0
AO–$Al_{48}Si_{52}$	0.4	20.0	14.6	13.9
AO–$Sn_{25}Al_{75}$	0.4	25.3	20.5	16.7

catalysts. The results of the AO-materials in the model esterification reaction are listed in Table 4. Ester yields between 91.4 and 97.4% were reached (calculated from the acid values). In general terms, the Sn/Si-oxides showed higher activities than the ternary Sn/Al/Si-oxides. The poorest result was achieved with the Sn/Al-combination, followed by the tin-free Al/Si-oxide. The highest ester yields were achieved with the AO–$Sn_{13}Si_{87}$ and AO–Sn_4Si_{96} samples.

Within the series of AO-materials, the following trends were observed. The specific B.E.T. surface area decreases in the order

$$\begin{aligned} \text{AO–Sn}_4\text{Si}_{96} &> \text{AO–Sn}_{13}\text{Si}_{87} > \text{AO–Sn}_{12}\text{Si}_{88} \\ &> \text{AO–Sn}_{25}\text{Al}_{75} > \text{AO–Sn}_{20}\text{Si}_{80} \\ &> \text{AO–Sn}_{25}\text{Al}_{36}\text{Si}_{39} > \text{AO–Al}_{48}\text{Si}_{52}, \end{aligned} \quad [1]$$

while the catalytic activity in the esterification reaction decreases in the order

$$\begin{aligned} \text{AO–Sn}_4\text{Si}_{96} &> \text{AO–Sn}_{13}\text{Si}_{87} > \text{AO–Sn}_{12}\text{Si}_{88} \\ &> \text{AO–Sn}_{20}\text{Si}_{80} > \text{AO–Sn}_{25}\text{Al}_{36}\text{Si}_{39} \\ &> \text{AO–Al}_{48}\text{Si}_{52} > \text{AO–Sn}_{25}\text{Al}_{75}. \end{aligned} \quad [2]$$

A correlation of activity with surface area and decreasing Sn content is found. From homogeneous catalysis with tin components it is known that the Lewis acidity is responsible for the catalytic activity (37). No obvious correlation of activity with Lewis acidity was found in the present work. The reuseability of the AO–Sn_4Si_{96} was investigated. The catalyst was reused twice without loss of activity. After separation of the catalyst particles (>0.4 μm), no Sn was detectable by ICP-AES (detection limit < 5 ppm) in the reaction mixture. Due to the autocatalytic nature of the basic reaction no rigorous proof of the heterogeneity of the catalysis was possible in this system.

Etherification

More information on the catalytic behaviour of the AO-catalysts was obtained with an acid catalyzed etherification reaction. The competition reaction of 1-hexanol and 1-naphthol with isobutene to the corresponding *t*-butylethers was studied to investigate the activity and shape selectivity of the AO catalysts in this addition reaction. The competitive etherification of both substrates, homogeneously catalyzed with mineral acids, leads to the preferred formation of naphthyl ether.

It was expected that the diffusion of the larger substrate molecule naphthol should be hindered in the small pores of the microporous AO catalysts favouring the formation of the hexylether. The results of the catalytic experiments are summarized in Table 5. Preferential formation of the hexylether was observed with AO–$Al_{48}Si_{52}$, AO–$Sn_{13}Si_{87}$, and AO–Sn_4Si_{96}. The reversed selectivity with AO–$Sn_{25}Al_{75}$ may be due to its larger pores identified in the physisorption studies. The catalytic activity in the etherification reaction decreases in the order

$$\begin{aligned} \text{AO–Sn}_4\text{Si}_{96} &> \text{AO–Al}_{48}\text{Si}_{52} > \text{AO–Sn}_{13}\text{Si}_{87} \\ &> \text{AO–Sn}_{25}\text{Al}_{75} > \text{AO–Sn}_{20}\text{Si}_{80} \\ &> \text{AO–Sn}_{25}\text{Al}_{36}\text{Si}_{39} > \text{AO–Sn}_{12}\text{Si}_{88}. \end{aligned} \quad [3]$$

There is no clear relationship between the physico-chemical properties of the AO materials [1, 2] and their catalytic activity.

The heterogeneity of the reaction was examined with the most active catalyst AO–Sn_4Si_{96}. In a typical etherification reaction, half the maximum conversion of the alcohols was reached after 1.5 h. At this time the catalyst was recovered from the liquid reaction solution and the run was continued without the catalyst. No further conversion of the alcohols was observed after the amorphous oxide was removed from the solution precluding homogeneous catalysis. Control experiments with the microporous silica AO–Si_{100} and without the catalyst showed trace conversion of naphthol compared with the metal-containing AO materials. Mixed oxides with a low concentration of Lewis acid sites, together with a high specific surface area, seem to be optimal for this etherification reaction.

TABLE 5

Comparison of Catalytic Etherification with AO-Materials

Sample	Conv. 1-hexOH [%]	Conv. 1-naphthol [%]
p-toluenesulfonic acid	59.4	100
AO–Sn_4Si_{96}	56.2	22.3
AO–$Al_{48}Si_{52}$	31.4	18.5
AO–$Sn_{13}Si_{87}$	15.6	4.3
AO–$Sn_{25}Al_{75}$	1.6	5.1
AO–$Sn_{20}Si_{80}$	1.5	1.7
AO–$Sn_{25}Al_{36}Si_{39}$	0.8	2.6
AO–$Sn_{12}Si_{88}$	0.5	1.3
AO–Si_{100}	0	1.3

Isomerization and Hydrocracking of Decane

Bifunctional catalysis involves a synergism of Brønsted acidity and hydrogenation–dehydrogenation activity provided, e.g. by platinum metal (38). Lewis acidity is much less effective in these hydrocarbon conversion reactions. Bifunctional catalysis can, therefore, be used to probe the Brønsted acidity of a solid. The decane conversion curves obtained on the various platinum-loaded AO materials are presented in Fig. 10. Literature data on a bifunctional zeolite catalyst (Pt/H-Y zeolite (39)) and an aluminophosphate molecular sieve (Pt/$AlPO_4$-5 (40)) are added for comparison. The AO samples are much less active than the Pt/H-Y zeolite. The conversion curves on the AO materials occur in the range of the platinum-loaded molecular sieve $AlPO_4$-5, which does not show any Brønsted acidity. These catalytic activities are consistent with the virtual absence of Brønsted activity in the AO materials according to the IR characterization with the pyridine probe (Fig. 8). The amorphous oxide containing a combination of silicon and aluminium AO−$Al_{48}Si_{52}$ is the most active sample investigated, although its specific surface area is very small (4 m^2/g, Table 1). Mixed oxides of silicon and aluminium exhibit Brønsted acidity of a weaker type than in zeolites (16).

To allow for a possible conversion of Lewis acid sites into Brønsted acid sites, the catalytic testing of the AO−$Sn_{20}Si_{80}$, AO−$Sn_{12}Si_{88}$, and AO−Sn_4Si_{96} was performed in the presence of additional water vapor (10 kPa) in the feed. No significant changes in the activity of the catalysts were observed, indicating that the Lewis acid sites present in the samples are rather weak and cannot be converted into Brønsted acid sites in the presence of water.

On all AO catalysts investigated, cracking was the most important reaction. Methane was the main reaction product, stemming from the hydrogenolysis of decane on the platinum and indicating an imbalance of the acid and metal catalytic functions. With the AO catalysts, the highest isomerization conversions obtained were in the range of 0.2 to 2%. Within the isomerization products, the methylnonanes are most abundant, and their distribution could be determined accurately. The methyl-branching selectivity of decane can be used to probe the micropore architecture of the catalyst (29, 41). The refined constraint index (CI°) is calculated as the ratio of the selectivities for 2-methylnonane versus 5-methylnonane formation at 5% decane isomerization conversion. Unfortunately, the 5% isomerization conversion level could not be reached for any of the AO samples, the main reaction being cracking. CI° values calculated at the highest isomerization conversions obtained are shown in Fig. 11. According to the CI° values, most of the samples behave like zeolites with pore diameters larger than 0.6 nm, i.e. large pore zeolites with pore openings circumscribed with 12 oxygen atoms (so-called 12-ring zeolites). One sample, AO−$Sn_{20}Si_{80}$, behaves like a material with pores that are smaller than 0.6 nm, i.e. the behaviour of a 10-ring zeolite. The decane test was found to be very effective for the characterization of other types of amorphous microporous mixed oxides, including titanosilicates and vanadosilicates. Excellent agreement of CI° values and pore sizes from physisorption experiments were obtained

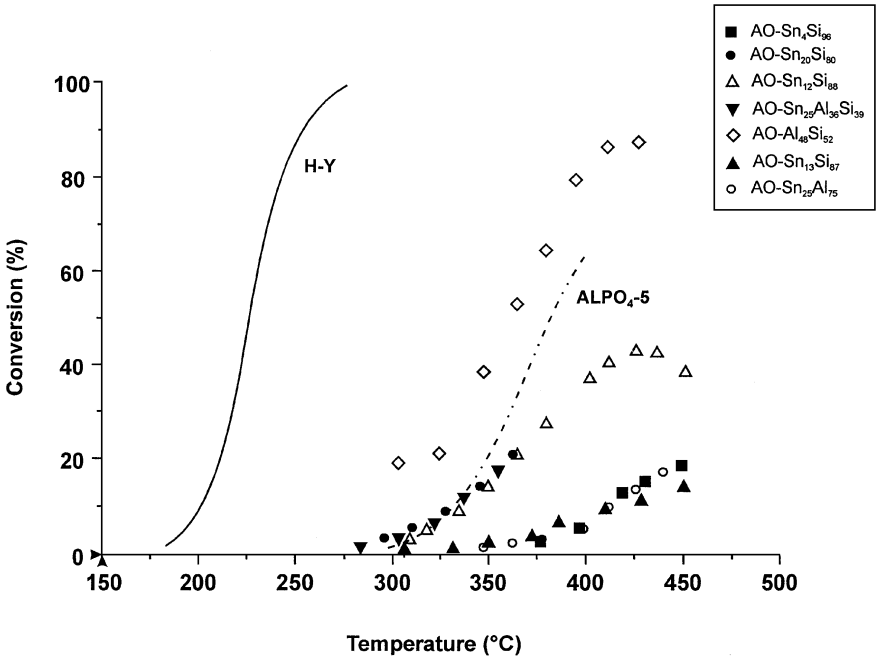

FIG. 10. Catalytic conversion of decane on the AO-catalysts.

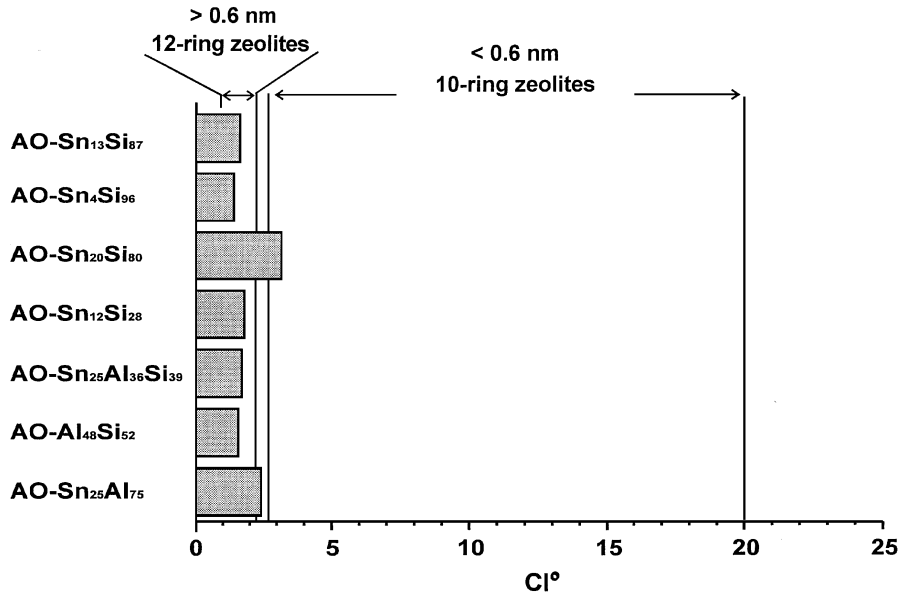

FIG. 11. CI° values of the AO-materials.

in the past (24). For the present series of stannosilicates and aluminates with very weak Brønsted acidity, the estimated pore sizes, according to the CI° criterion, do not agree well with the argon adsorption experiments (compare Table 1 and Fig. 11). For instance, for the AO–$Sn_{20}Al_{80}$ sample, the CI° criterion predicts pores smaller than 0.6 nm (Fig. 11) compared to 0.7 nm according to argon physisorption (Table 1). Owing to the very weak Brønsted acidity and the imbalance of the catalytic functions, the decane test is not as appropriate for a precise estimation of pore sizes in these types of samples.

CONCLUSIONS

Amorphous Sn-, Si-, Al-containing mixed oxides with homogeneous elemental distribution, as well as elemental domains and well-characterized pore architecture, including micropores and mesopores, were prepared under controlled conditions using two different sol–gel processes. It was found that the Sn–Si-mixed oxides with low Sn content are very active and selective mild acid catalysts that are useful for esterification and etherification reactions. These materials have large surface areas, and their catalytic activities and selectivities are excellent. Substitution of silicon by aluminum shows the expected increase in activity in the decane test, where Brønsted sites are required, but it was found that larger Sn contents or the presence of Al centers decrease the catalytic performance in esterification reactions. It is shown by pyridine adsorption, infrared spectroscopy, decane isomerization, and hydrocracking experiments that these amorphous stannosilicates are Lewis acidic and show no, or very weak Brønsted acidity. The Lewis acidity in the samples is probably responsible for the catalytic activity in esterification and etherification reactions. In the esterification reaction of pentaerythritol and stearic acid there are correlations of catalytic activity with surface area and decreasing tin content. The trend with decreasing tin content points to the potential importance of isolated Sn centers as active sites. This study indicates that this scientific search for new mildly acidic solid catalysts was successful and may be beneficial for a large range of chemical reactions involving homogeneous acid catalysis.

ACKNOWLEDGMENTS

This collaboration was initiated by the Concerted European Action: "Sol–Gel Processing for Advanced Industrial Material Technologies." We thank the European Action for contributing to travel expenses and meetings. J.A.M. acknowledges the Flemish F.W.O. for a research position, W.S. thanks the Flemish I.W.T., and S.S. thanks the MPG for a fellowship. We also thank W. Ben Mustapha for the etherification experiments and H. Bretinger of MPI for sorption analyses.

REFERENCES

1. Izumi, Y., Urabe K., and Onaka, M., "Zeolite, Clay and Heteropoly Acid in Organic Reactions." VCH Verlagsgesellschaft, Weinheim, 1992.
2. Arata, K., *Trends Phys. Chem.* **2**, 1 (1991).
3. Corma, A., *Chem. Rev.* **95**, 559 (1995).
4. Yadav, G., and Mekta, P., *Ind. Eng. Chem. Res.* **33**, 2198 (1994).
5. Thorat, T., Yadav, V., and Yadav, G., *Appl. Catal. A* **90**, 73 (1992).
6. Misono, M., and Okuhara, T., *Mat. Res. Soc. Symp. Proc.* **368**, 215 (1995).
7. Patel, A., Coudurier, G., Essayem, N., and Védrine, J. C., *J. Chem. Soc. Faraday Trans.* **93**, 347 (1997).
8. Wang, G.-W., Hattori, H., and Tanabe, K., *Chem. Lett.*, 277 (1983).
9. Itoh, M., Hattori, H., and Tanabe, K., *J. Catal.* **43**, 192 (1976).
10. Hino, M., and Arata, K., *Chem. Lett.*, 1737 (1990).
11. Matsuhashi, H., Hino, M., and Arata, K., *Appl. Catal.* **59**, 205 (1990).

12. Lu, G., *Appl. Catal. A* **133**, 11 (1995).
13. Harrison, P. G., and Azelee, W., *J. Sol–Gel Sci. Technol.* **2**, 813 (1994).
14. Tanabe, K., *in* "Catalysis Science and Technology" (J. A. Anderson and U. Bondart, Eds.), Vol. 2, p. 231. Springer-Verlag, Berlin, 1982. [Kung, H. H., *Stud. Surf. Sci. Catal.* **45**, 73 (1989)]
15. Tanabe, K., Misono, M., Ono, Y., and Hattori, H., *Stud. Surf. Sci. Catal.* **51** (1989).
16. Gajada, G. J., and Rabo, J. A, *in* "Acidity and Basicity of Solids" (J. Fraissard and L. Petrakis, Eds.), p. 127. Kluwer Academic, Norwell, MA, 1994.
17. Brinker, C. J., and Scherrer, G. W., "Sol–Gel Science. The Physics and Chemistry of Sol–Gel-Processing." Academic Press, New York, 1990.
18. Hench, L. L., and West, J. K., *Chem. Rev.* **90**, 33 (1990).
19. Perry, C. C., Harrison, P. G., Li, X., and Creaser, D. A., *in* "Eurogel '91" (S. Vilminot, R. Nass, and H. Schmidt, Eds.), pp. 175, 187. Elsevier, Amsterdam, 1992.
20. Carturan, G., Ceccato, R., Principi, G., and Russo, U., *J. Radioanal. Nucl. Chem.* **190**, 419 (1995).
21. Catruran, G., Ceccato, R., Campostrini, R., and Sglavo, V. M., *J. Sol–Gel Sci. Technol.* **5**, 57 (1995).
22. Catruran, G., Ceccato, R., and Campostrini, R., *J. Sol–Gel Sci. Technol.* **5**, 49 (1995). [Maschio, R. D., Dire, S., Campostrini, R., Soraru, G. D., and Carturan, G., *Mat. Res. Soc. Symp. Proc.* **180**, 351 (1990)]
23. Klein, S., Thorimbert, S., and Maier, W. F., *J. Catal.* **163**, 476 (1996).
24. Maier, W. F., Martens, J. A., Klein, S., Heilmann, J., Parton, R., Vercruysse, K., and Jacobs, P. A., *Angew. Chem., Int. Ed. Engl.* **35**, 180 (1996).
25. Maier, W. F., Tilgner, I.-C, Wiedorn, M., and Ko, H.-C., *Adv. Mater.* **5**, 726 (1993).
26. Kishor Mal, N., Ramaswamy, V., Ganapathy, S., and Ramaswamy, A. V., *Appl. Catal. A* **125**, 233 (1995).
27. Kishor Mal, N., Ramaswamy, V., Ganapathy, S., and Ramaswamy, A. V., *J. Chem. Soc., Chem. Commun.*, 1933 (1994).
28. Chavan, S., Zubaidha, P., Dantale, S., Keshavaraja, A., Ramaswamy, A., and Ravindranathan, T., *Tetrahedron Lett.* **37**, 233 (1996).
29. Martens, J. A., Tielen, Jacobs, P. A., and Weitkamp, J., *Zeolites* **4**, 98 (1984).
30. Lowell, S., and Shields, J. E., "Powder surface area and porosity." Chapma & Hall, London, 1991. [Venero, A. F., and Chiou, J. N., *in* "Microstructure and Properties of Catalysts; Mat. Res. Sym. Proc." (M. M. J. Treacy *et al.*, Eds.), Vol III, p. 235, MARS, Pennsylvania, 1988.]
31. Horvath, G., and Kawazoe, K., *J. Chem. Eng. Jpn.* **16**, 470 (1983).
32. Hathaway, P. A., and Davis, M. T., *Catal. Lett.* **5**, 333 (1990).
33. Cotterman, R. L, Hickson, D. A., Cartlidge, S., Dybowski, C., Tsiao, C., and Venero, A. F., *Zeolites* **11**, 27 (1991).
34. Knözinger, H., *in* "Elemental Reaction Steps in Heterogeneous Catalysis" (R. W. Joyner and R. A. van Santen, Eds.), p. 267. Kluwer Academic, Norwell, MA, 1993.
35. Jacobs, P. A., *in* "Characterization of Heterogeneous Catalysts" (F. Delannay, Ed.), p. 367. Dekker, New York, 1984.
36. Harrison, P. G., "Chemistry of tin." Chapman & Hall, New York, 1989.
37. Taube, R., "Homogene Katalyse." Akad. Verlag, Berlin, 1988.
38. Coonradt, M. L., and Garwood, W. E, *Ind. Eng. Chem. Prod. Res. Dev.* **3**, 38 (1964).
39. Martens, J. A., Balakrishnan, L., Grobet, P. J., and Jacobs, P. A., *Stud. Surf. Sci. Catal.* **69**, 135 (1991).
40. Martens, J. A., Uytterhoeven, L., Jacobs, P. A., and Froment, G. F., *Stud. Surf. Sci. Catal.* **75**, 2829 (1992).
41. Jacobs, P. A., and Martens, J. A., *Pure Appl. Chem.* **58**, 1329 (1986).